Electronic Supplementary Material (ESI) for Chemical Science.

Supplementary Information

Manganese vacancy-confined single-atom Ag in cryptomelane nanorods for efficient Wacker oxidation of styrene derivatives

Hongling Yang,[a] Xun Zhang,[c] Yi Yu,[c] Zheng Chen,[d] Qinggang Liu,[a] Yang Li,[a] Weng-Chon Cheong,[e] Dongdong Qi,[f] Zewen Zhuang,[a] Qing Peng,[a] Xin Chen,[b],* Hai Xiao,[a] Chen Chen,[a],* and Yadong Li[a]

[a]Department of Chemistry, Tsinghua University, Beijing 100084, China

[b]Beijing Advanced Innovation Center for Materials Genome Engineering, Institute of Solid State Chemistry, University of Science and Technology Beijing, Beijing 100083, China

[c]School of Physical Science and Technology, Shanghai Tech University, Shanghai 201210, China

[d]College of Chemistry and Materials Science, Anhui Normal University, Wuhu 241000, China

[e]Department of Physics and Chemistry, Faculty of Science and Technology, University of Macau, Taipa, Macau SAR, 999078, China

[f]Beijing Key Laboratory for Science and Application of Functional Molecular and Crystalline Materials, Department of Chemistry, University of Science and Technology Beijing, Beijing 100083, China

Experimental Section

Synthesis of Ag_1/OMS-2 and OMS-2. In a typical synthesis of Ag_1/OMS-2, 0.315g of $AgNO_3$ was initially dissolved in 20 mL deionized water to form a solution, to which ammonia (25 wt.%) was slowly added under stirring until the solution became clear to give a transparent $[Ag(NH_3)_2]OH$ solution. Subsequently, both the $[Ag(NH_3)_2]OH$ solution and a H_2O_2 solution (30 wt.%) were respectively and simultaneously added to another suspension (100 mL) containing the OMS-2 (2.000 g) under stirring at 0 °C for 0.5 h. The final suspension was filtered, washed with distilled water, and then dried in 120 °C for 24 h, followed by annealing at 500 °C in air for 6 h. OMS-2 was prepared with the same synthesis procedure of Ag_1/OMS-2 except $AgNO_3$ was not added.

Synthesis of Ag NPs/OMS-2. The Ag NPs/OMS-2 sample with the same amount of Ag as the Ag_1/OMS-2 sample was prepared by impregnating the OMS-2 powder with an aqueous solution of $AgNO_3$, and then dried at 120 °C for 24 h and calcined at 500 °C in air for 6 h.

Characterization. *Positron Annihilation Spectroscopy*. The positron lifetime experiment was performed on the positron research platform of the Institute of High Energy Physics, Chinese Academy of Sciences. The positron lifetime experiments were carried out with a fast-slow coincidence ORTEC system with a time resolution of about 195 ps full width at half-maximum. The positron annihilation lifetime spectrometer uses a pair of BaF_2 scintillator detectors to detect gamma rays released after positron annihilation. A ^{22}Na positron source was sandwiched between two identical samples, and the total count was two million. The LT9.0 software was employed to unpack the spectrum. The measurement system electronics plug-in is the standard NIM plug-in of EG&G in the United States.

Data analysis. The experimental positron lifetime spectrum can be expressed as the convolution of the preferably Gaussian resolution function *R(t)* with the sum of exponential functions:[1]

$$N(t) = \int_{-\infty}^{\infty} ds R(s) \left(-\frac{dn}{dt}(t-s) \right)$$

The fitting parameters include the FWHM of the resolution function and the intensities I_i and annihilation rates λ_i (slopes on the semilogarithmic plot) of the lifetime components. The subtraction of source components is performed prior to final analysis of the data.

TEM images were obtained on a Hitachi H-800 TEM operated at 100 kV. HAADF−STEM images were obtained on a Titan Themis 60-300 STEM operated at 300 kV, equipped with a spherical probe aberration corrector. XPS was performed on an ULVAC PHI Quantera microscope. XRD data were measured on a Rigaku RU-200b with Cu Kα radiation (λ = 1.5406 Å). O_2-TPD was conducted in a Micromeritics Chemisorb 2720 apparatus. Raman measurements were performed on a LabRAM HR Evolution apparatus (HORIBA Jobin Yvon). The metal concentration measurement was conducted by ICP-OES (Optima 2000DV, Perkin Elmer).

Structure modeling and HAADF−STEM image simulation. We prepared two models for image simulation by randomly doping seven Ag atoms in Mn positions, and another case with three Ag atoms located in the spacing between Mn columns. HAADF−STEM image simulations were performed using a plane wave reciprocal space interpolated scattering matrix (PRISM) method.[2] The accelerating voltage is 300 kV, and the interpolation factor we used is 5. The maximum α convergence angle is 25 mrad, and the probe α and collection angles were set at 25 mrad and 75−200 mrad, respectively. In order to get closer to the experimental data. Poisson white noise was added to the simulated images (Fig. S4). Structure models shown in this work were drawn using VESTA software.[3]

XAFS measurements. The X-ray absorption fine structure spectra data (Ag *K*-edge, Mn *K*-edge) were collected at the BL14W1 station in Shanghai Synchrotron Radiation Facility (SSRF, 3.5 GeV, 250 mA maximum, Si(311) double crystals), the O *K*-edge XAFS spectra were collected at BL12B station of National Synchrotron Radiation Laboratory (NRSL) in Hefei. The XAFS data of the Ag_1/OMS-2 and all of the references (metal powder, foils and oxide bulks) were recorded in the transmission mode using an ionization chamber at room temperature. All of the samples were pelletized as disks 13 mm in diameter with 1 mm thicknesses.

XAFS analysis and results. The acquired EXAFS data were processed according to standard procedures using the ATHENA module implemented in the IFEFFIT software packages.[4,5] The EXAFS spectra were obtained by subtracting the post-edge background from the overall absorption and then normalizing with respect to the edge-jump step. Then, χ(k) data in the *k*-space were Fourier transformed to real (R) space using Hanning windows (dk = 1.0 Å^{-1}) to separate the EXAFS contributions from different coordination shells. The quantitative information can be obtained by the least-squares curve fitting in the R space using the module ARTEMIS of programs of IFEFFIT. The following EXAFS equation was used:

$$\chi(k) = \sum_j \frac{N_j S_0^2 F_j(k)}{k R_j^2} \exp[-2k^2 \sigma_j^2] \exp[\frac{-2R_j}{\lambda(k)}] \sin[2k R_j + \Phi_j(k)]$$

Where S_0^2 is the amplitude reduction factor, $F_j(k)$ is the effective curved-wave backscattering amplitude, N_j is the number of neighbors in the j^{th} atomic shell, R_j is the distance between the X-ray absorbing central atom and the atoms in the j^{th} atomic shell (backscatterer), λ is the mean free path in Å, $\phi_j(k)$ is the phase shift (including the phase shift for each shell and the total central atom phase shift), σ_j is the Debye-Waller parameter of the j^{th} atomic shell (variation of distances around the average R_j). The functions $F_j(k)$, λ and $\phi_j(k)$ were calculated with the ab initio code FEFF8.2.

The Ag *K*-edge theoretical XANES calculations were carried out with the FDMNES code in the framework of the real-space full multiple scattering (FMS) scheme using the muffin-tin approximation for the potential.[6,7] The energy dependent exchange-correlation potential was calculated in the real Hedin–Lundqvist scheme, then the spectra were convoluted using a Lorentzian function with an energy-dependent width to account for the broadening due to the corehole width and the final state width.

The O *K*-edge Near Edge X-ray Absorption Fine Structure (NEXAFS) were carried out at the Catalysis and Surface Science Endstation at the BL11U beamline in the National Synchrotron Radiation Laboratory (NSRL) in Hefei, China. This beamline is connected to an undulator and equipped with two gratings that offer soft X-rays of 600 eV with a typical photon flux of 5×1010 photons/s and a resolution (E/ΔE) better than 105 at 29 eV. This system is comprised of four ultrahigh vacuum (UHV) chambers including analysis chamber, preparation chamber, molecular beam epitaxy (MBE) chamber, and a radial distribution chamber. The base pressures are 7×10^{-11}, 1×10^{-10}, 5×10^{-10} and 2×10^{-11} mbar, respectively. A sample load-lock system is connected to the sample transfer chamber. The analysis chamber is equipped with a VG Scienta R4000 analyzer, a monochromatic Al *K*a X-ray source, a UV light source, low energy electron diffraction (LEED), a flood electron gun, and a manipulator with high precision and five-degree-of-freedom. The preparation chamber comprises an ion gun, a quartz crystal microbalance (QCM), a residual gas analyzer, a manipulator with high precision and four-degree-of-freedom, and several evaporators. The MBE chamber houses a QCM, several evaporators and a manipulator with two-degree-of-freedom. With this radial distribution chamber, the time for each transfer process between two chambers is less than 1 minute.

Catalysis testing. Typically, the Wacker oxidation of alkenes was carried out in a 100 mL sealed round bottom flask equipped with a reflux condenser. In a typical procedure, 10.5 mmol of styrene and 15 mmol of tert-butyl hydroperoxide (TBHP) were added to a mixture of 20 mg of catalyst and 20 mL of acetonitrile in the flask under stirring at 80 °C for 10 h. Given that tert-butyl hydroperoxide will decompose rapidly, so the temperature is raised slowly to the desired reaction temperature. After centrifugation, the products of the reaction were analyzed by gas chromatography (GC) and gas chromatography-Mass Spectrometer (GC-MS). The GC analysis was conducted on a Thermo Trace1300 series GC with an FID detector using a capillary column (TG-5MS, from Thermo Scientific, length 30 m, i.d. 0.25 mm, film 0.25 μm). The GC-MS analysis was carried out on a ISQ GC-MS with a ECD detector (Thermo Trace GC Ultra) using a capillary column (TG-5MS, from Thermo Scientific, length 30 m, i.d. 0.25 mm, film 0.25 μm). ^{1}H NMR and ^{13}C NMR data were recorded with a Bruker Advance III (400 MHz) spectrometer.

Calculation of turnover frequency (TOF). The TOF value was calculated according to the previous report,[8] and the detail was described as below:

$$\text{TOF} = \frac{\text{Total styrene turnovers}}{\text{Active sites} \times \text{Time}}$$

The number of total styrene turnovers was calculated based on the change of styrene concentration before and after reaction, which were determined by GC and GC-MS, following the equation:

$$\begin{aligned}\text{Total styrene turnovers} &= n_{\text{styrene}} \times \text{Conversion}\\ &= 10.5\text{ mmol} \times 10\%\\ &= 1.05\text{ mmol}\end{aligned}$$

The number of active sites in Ag_1/OMS-2 catalyst was calculated from the mass loading on the OMS-2 support, the Ag contents and the Ag atomic weight. All Ag atoms in Ag_1/OMS-2 are counted as active sites to calculate the TOF value:

$$\text{Active sites} = \frac{\text{Catalyst mass} \times \text{Catalyst loading} \times \text{Ag dispersity}}{M_{\text{Ag}}}$$

$$= \frac{20\ \text{mg} \times 2.5\% \times 100\%}{108\ \text{g/mol}}$$

$$= 4.6 \times 10^{-3}\ \text{mmol}$$

Finally, calculation of the TOF value was based on the following formula:

$$\text{TOF} = \frac{1.05\ \text{mmol}}{4.6 \times 10^{-3}\ \text{mmol} \times 0.22\ \text{h}}$$

$$= 1038\ \text{h}^{-1}$$

STEM simulation details

Simulation process
Case 1: Ag atoms substitute Mn atoms

Step 1

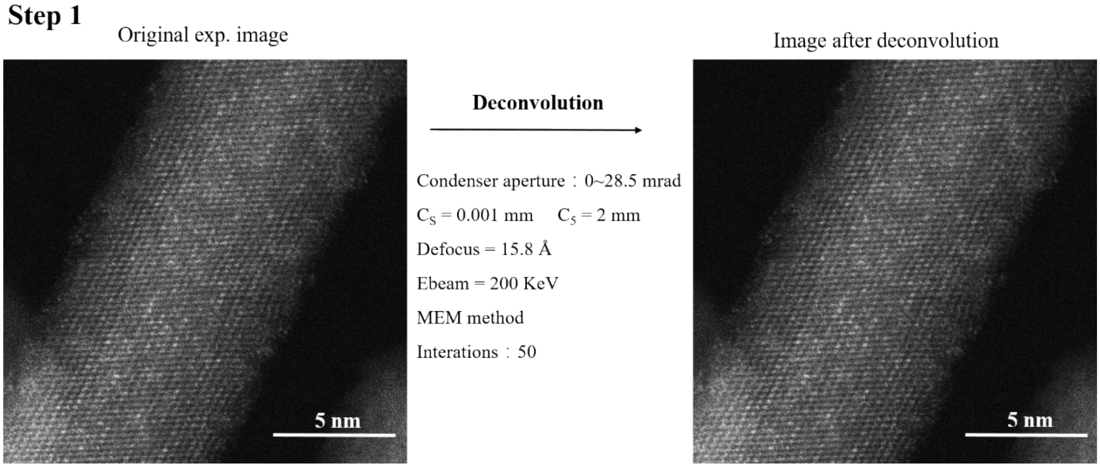

Condenser aperture：0~28.5 mrad

C_S = 0.001 mm C_5 = 2 mm

Defocus = 15.8 Å

Ebeam = 200 KeV

MEM method

Interations：50

Step 2

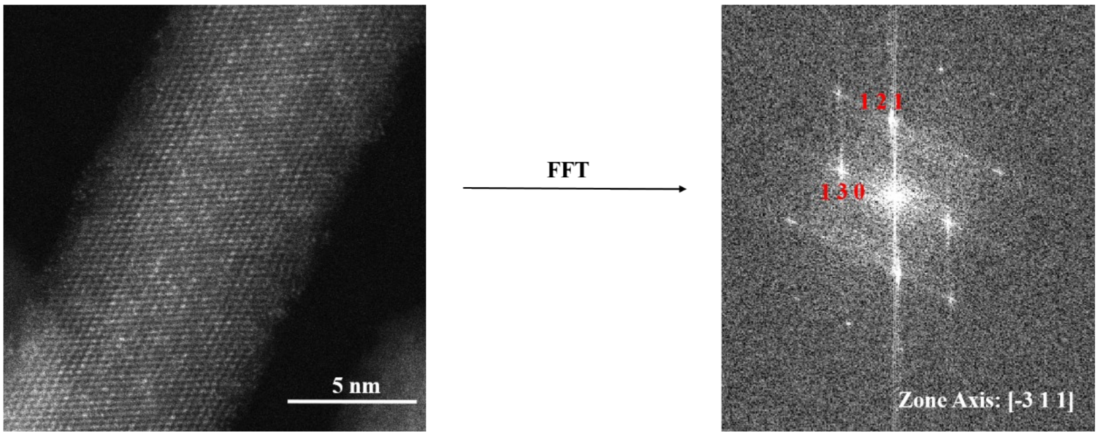

Step 3

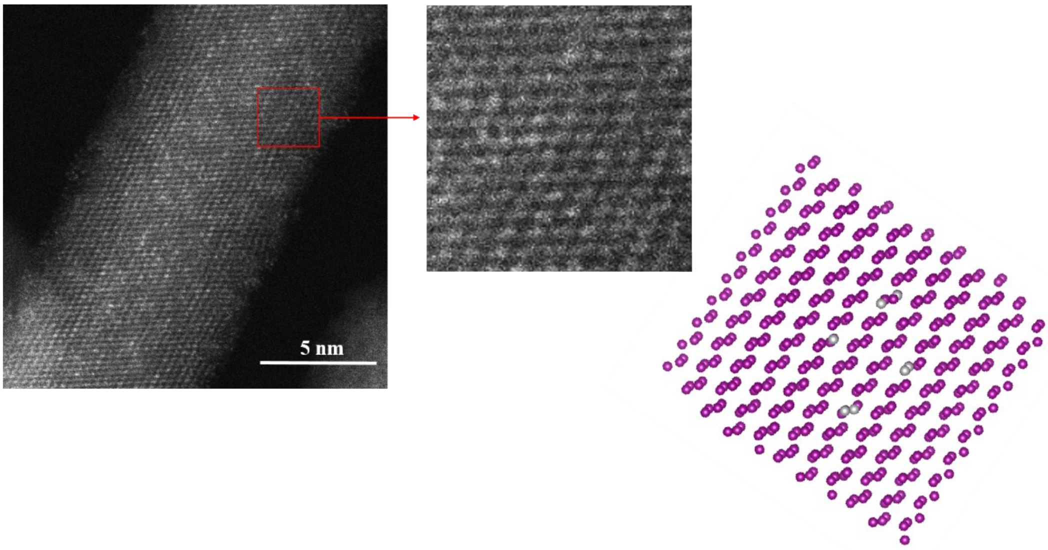

Step 4

Model

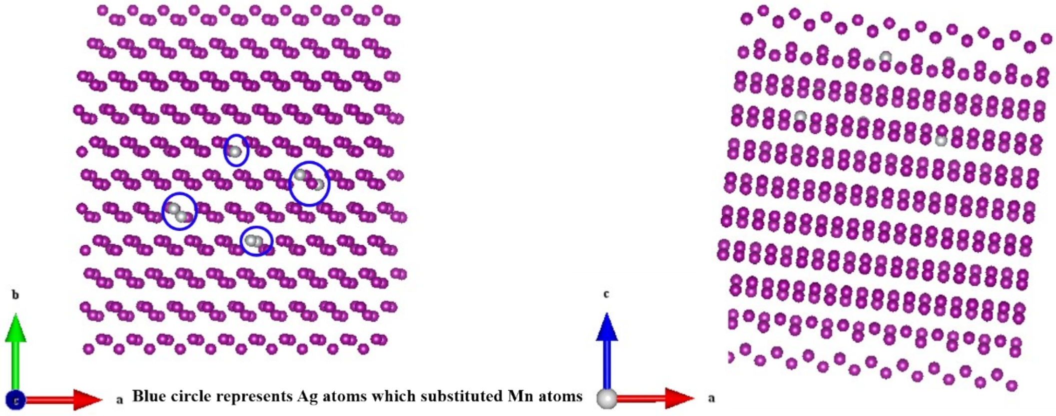

Blue circle represents Ag atoms which substituted Mn atoms

Simulation results

1. STEM simulation image

Parameters of STEM simulation:
pixel size: 0.05 pixel/Å
frozen phonon: 1
Thickness of slice: 3.42 Å
Interpolation Factor: 5
Microscope voltage: 200 KV
Maximum alpha angle: 28.5 mrad
Probe alpha angle: 28.5 mrad
collection angle：75 - 120 mrad

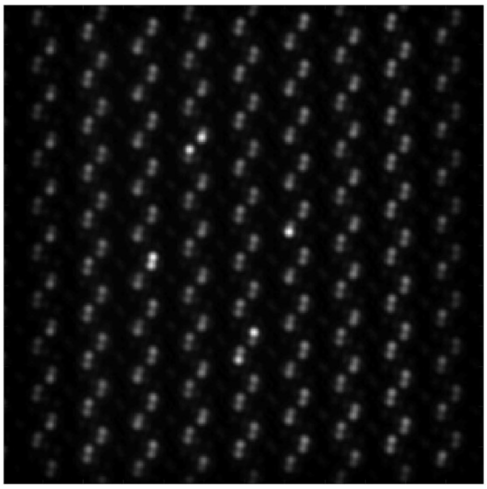

2. STEM simulation image added convolution

Parameters of convolution:
Microscope voltage: 200 kV
spherical aberration: 0.001 mm
Defocus: 15.8 Å
Objective aperture semiangle: 28.5 mrad
Source size: 0.6 Å^{1}
Size of slice: 29.86 Å
Number of pixels: 1078

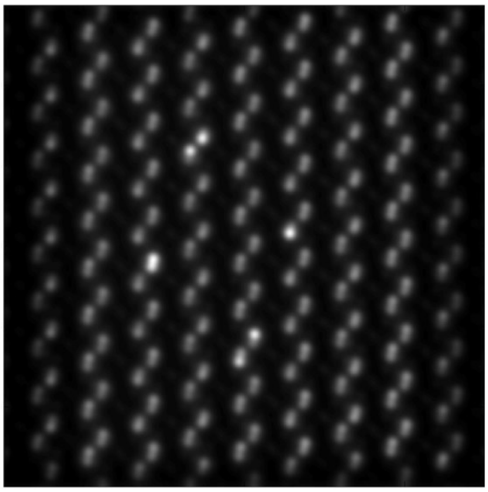

3. STEM simulation image added Poisson noise

Counts = 20

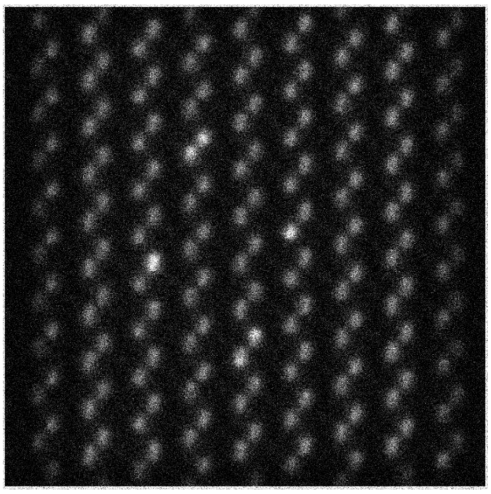

Case 2: Ag atoms locate in the spacing between Mn columns

Models

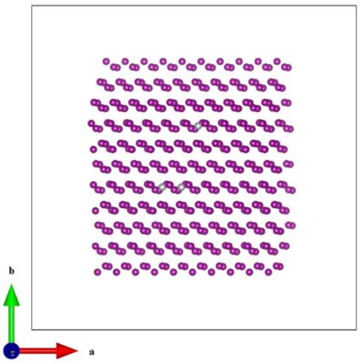

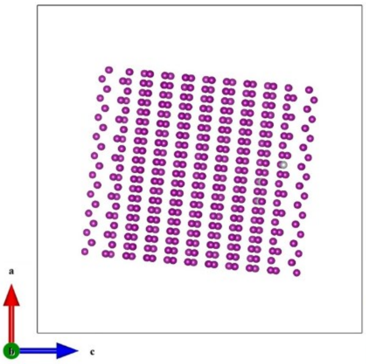

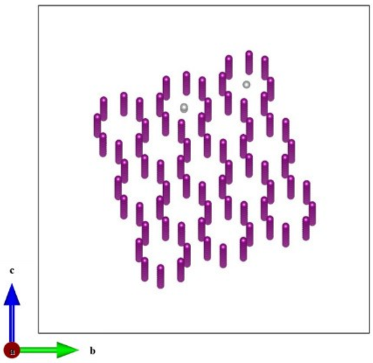

Simulation results

1. STEM simulation image

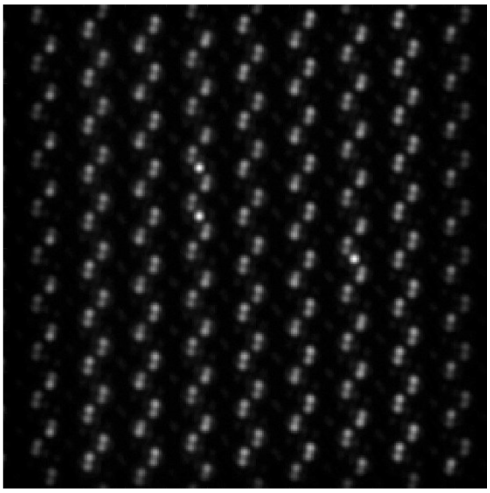

Parameters of STEM simulation:
pixel size: 0.05 pixel/Å
frozen phonon: 1
Thickness of slice: 3.42 Å
Interpolation Factor: 5
Microscope voltage: 200 KV
Maximum alpha angle: 28.5 mrad
Probe alpha angle: 28.5 mrad
collection angle : 75 - 120 mrad

2. STEM simulation image added convolution

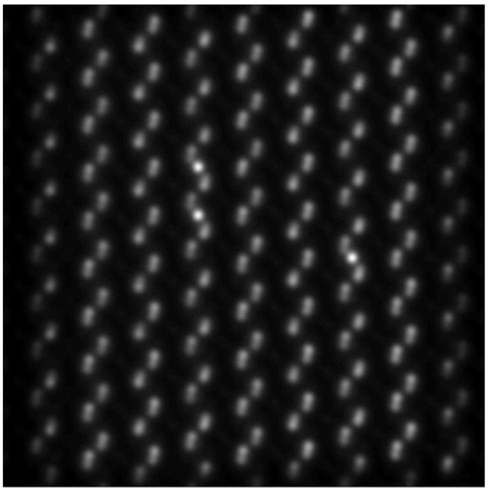

Parameters of convolution:
Microscope voltage: 200 kV
spherical aberration: 0.001 mm
Defocus: 15.8 Å
Objective aperture semiangle: 28.5 mrad
Source size: 0.6 Å[1]
Size of slice: 29.86 Å
Number of pixels: 1078

3. STEM simulation image added Poisson noise

Counts = 20

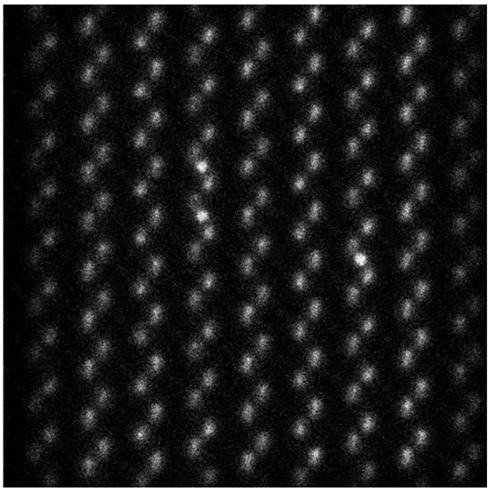

Computational details

In an attempt to understand the synergistic effect, density functional theory (DFT) calculations were carried out via Vienna ab initio simulation package (VASP)[9,10] program by using projected augmented wave (PAW) potential[11] and the Perder-Burke-Ernzergof (PBE) functional within the formulation of generalized gradient approximation (GGA).[12,13] The cutoff energy for the plane-wave expansion was set to 400 eV. The energy convergence criteria for electronic self-consistent loop was set to 10^{-5} eV, and the residual force on each atom was smaller than 0.02 eV/Å for structural relaxations. To investigate the substituted Ag atoms on the surface of OMS-2, we use the four-layer OMS-2 with 4×4 supercell to avoid the interaction between the replicas due to the periodic boundary conditions. A vacuum level of 15 Å was set to avoid interactions between periodic slabs. The reciprocal space was sampled by the gamma point in the Brillouin zone with a grid of 1×1×1. The harmonic frequency analysis of each optimized structure at the same level was carried out to verify that the stationary points exhibit no imaginary frequency while the transition states exhibit one imaginary frequency.

The formation energies of substituted Ag on OMS-2 slab were calculated using the following equation:

$$E_f = E_{sub} - E_{slab} - E_{Ag} + E_{Mn}$$

Where E_{sub} is the total energy of substrate substituted with Ag atoms, E_{slab} is the energy of unsubstituted OMS-2 substrate. The energy for Ag (E_{Ag}) is calculated from Ag bulk with the space group of R3m. E_{Ag} is the total energy of the Ag bulk divided by the total number of Ag atoms. E_{Mn} is calculated in the same method from Mn bulk with the space group of I43m. A gamma-centered (8 × 8 × 8) k-point grid was used for the (2 × 2 × 2) supercell of Ag and Mn bulks, and the width of smearing is set as 0.2 eV. The energy convergence criteria are in consistent with the calculation for OMS system.

The method used for the minimum energy paths and related energies is the projector augmented wave (PAW) method, of the same parameters with structure relaxations. The energy convergence criterion was set to 10^{-5} eV for self-consistent loop, and the residual force on each atom was smaller than 0.01 eV/Å, also the same with structure optimization.

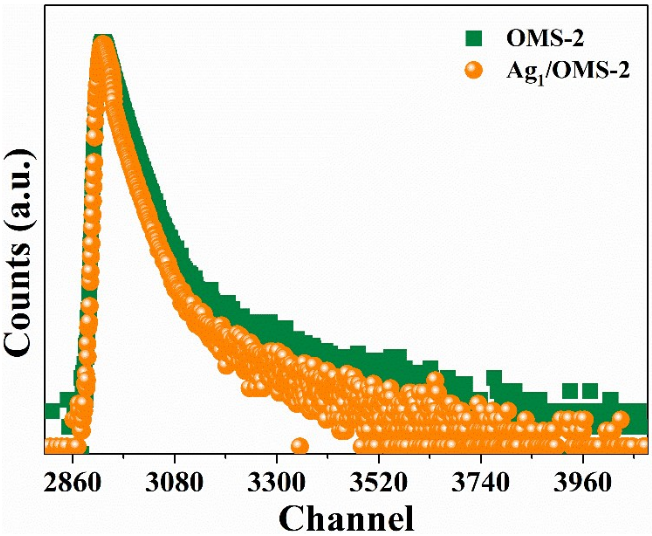

Fig. S1 The Positron lifetime spectra of OMS-2 and Ag_1/OMS-2.

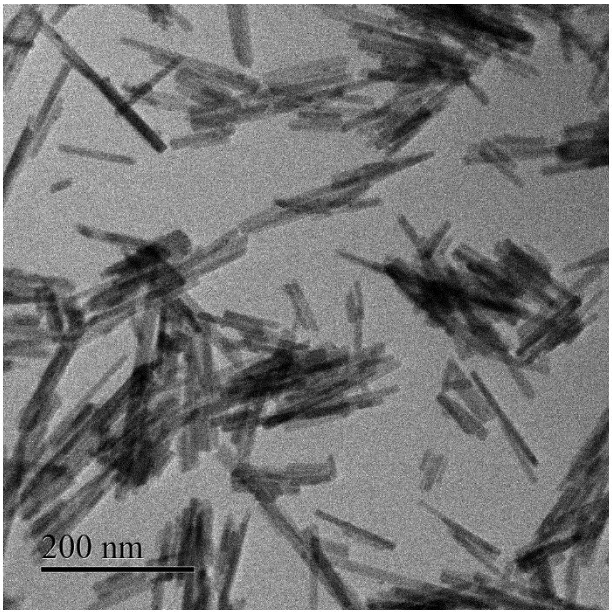

Fig. S2 TEM image of OMS-2 nanorods.

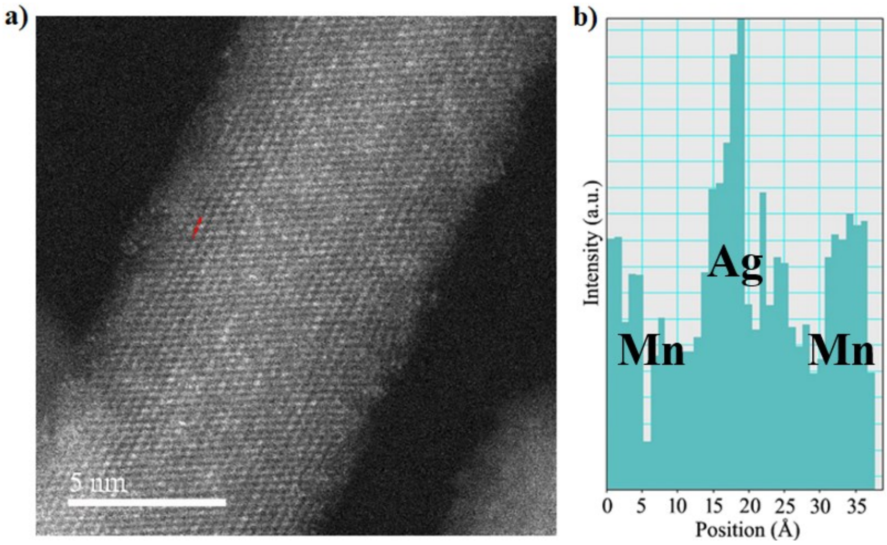

Fig. S3 a HAADF−STEM image of Ag_1/OMS-2 and **b** corresponding intensity maps obtained in the red line of (**a**).

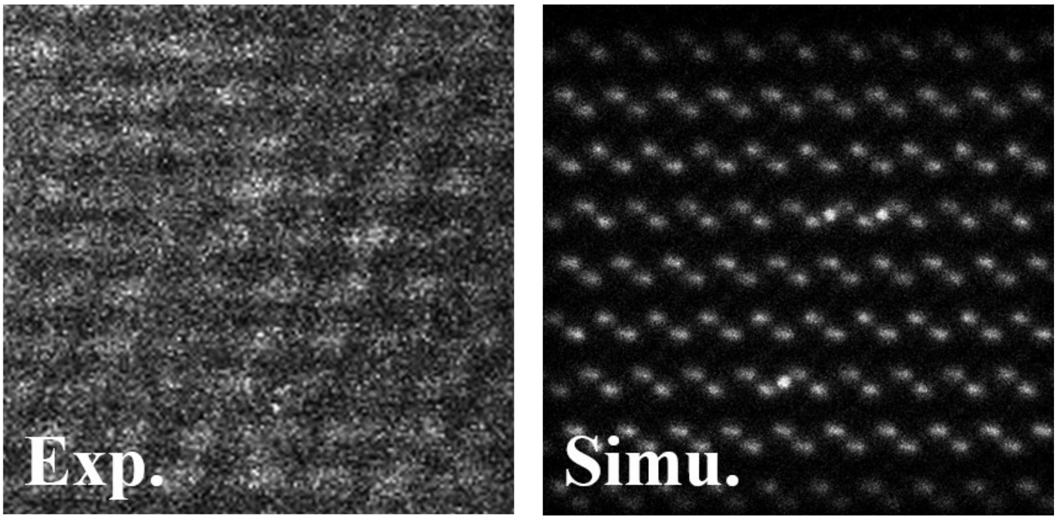

Fig. S4 Experimental HAADF−STEM image and simulated HAADF−STEM image using a model with three Ag atom located in the spacing between Mn columns.

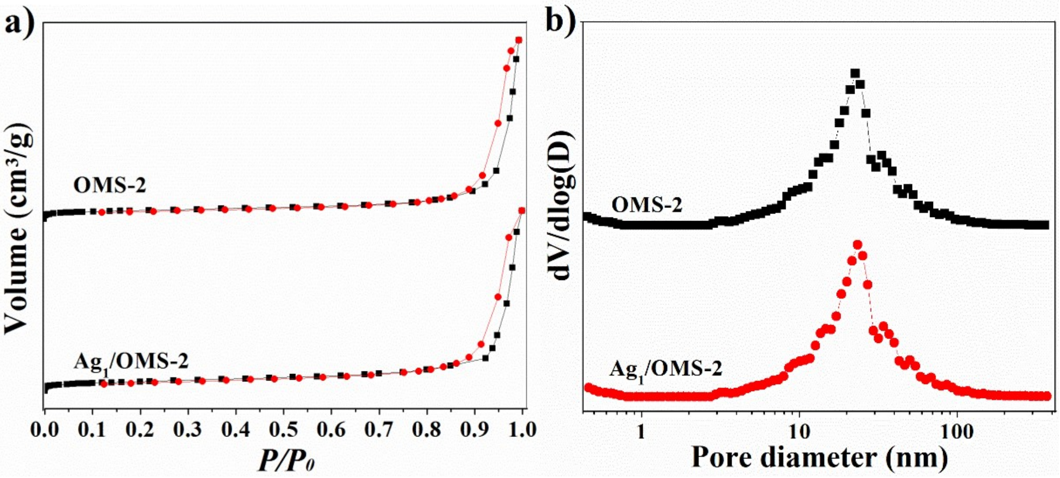

Fig. S5 **a** N_2 adsorption-desorption isotherms and **b** pore size distribution curves for OMS-2 and Ag_1/OMS-2.

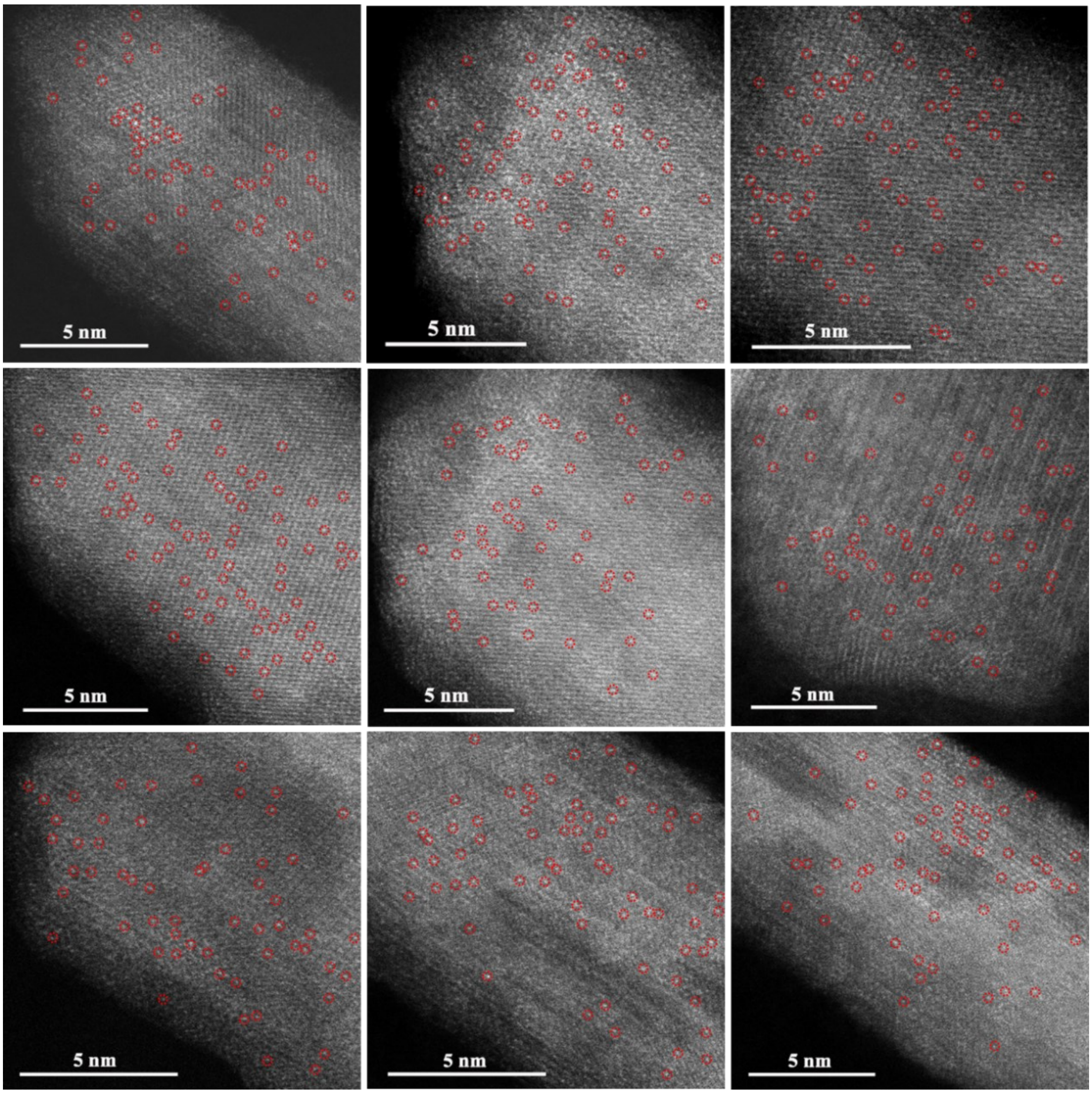

Fig. S6 AC HAADF-STEM images of Au$_1$/OMS-2, metal single atoms are highlighted with red circles.

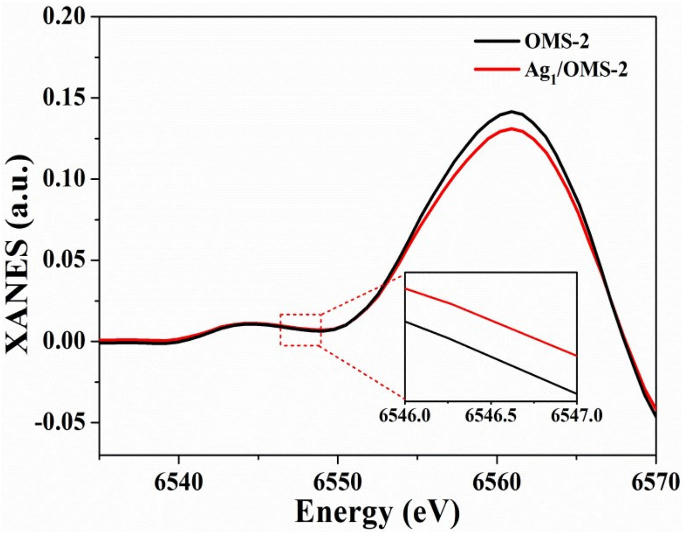

Fig. S7 Mn *K*-edge XANES spectra of OMS-2 and Ag_1/OMS-2.

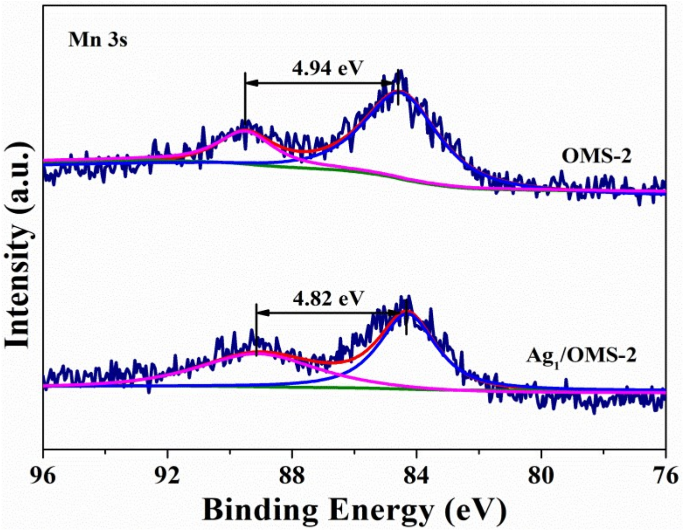

Fig. S8 Mn 3*s* XPS spectra of OMS-2 and Ag_1/OMS-2.

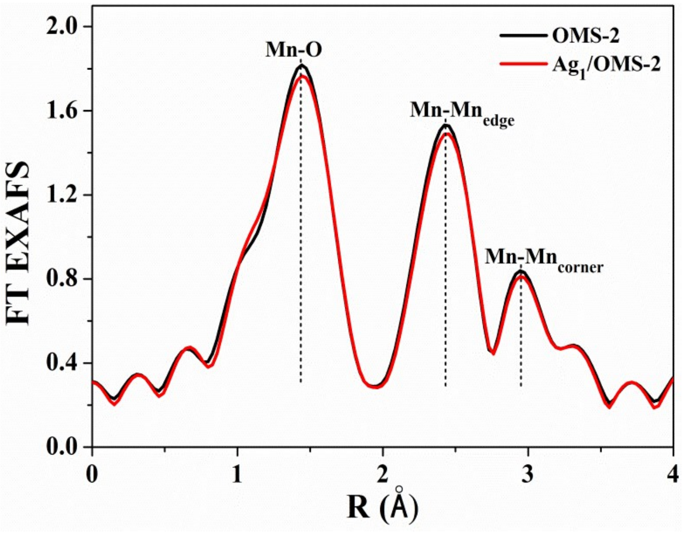

Fig. S9 EXAFS FT spectra at the Mn *K*-edge of OMS-2 and Ag_1/OMS-2.

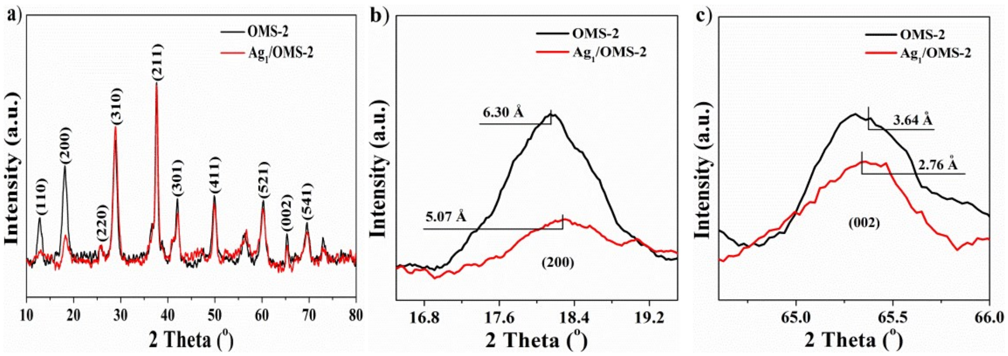

Fig. S10 a XRD patterns and **b,c** Lattice parameters of a and c calculated from the (200) and (002) diffraction peaks of OMS-2 and Ag_1/OMS-2, respectively.

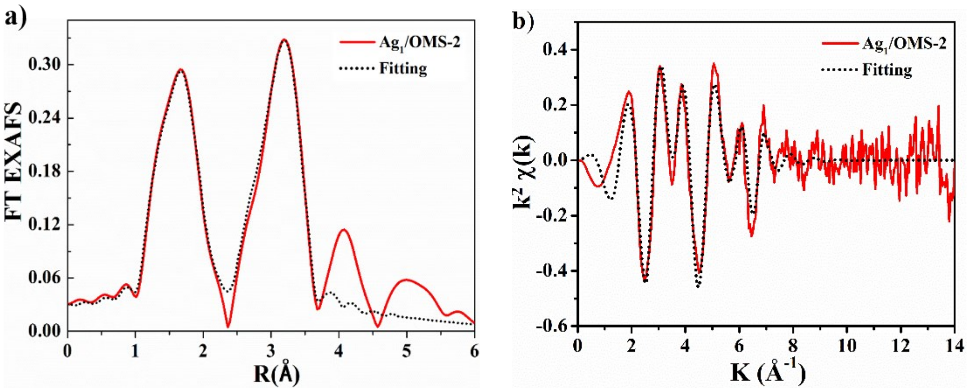

Fig. S11 Corresponding fits of the EXAFS spectrum of Ag_1/OMS-2 in **a** R space and **b** K space, respectively.

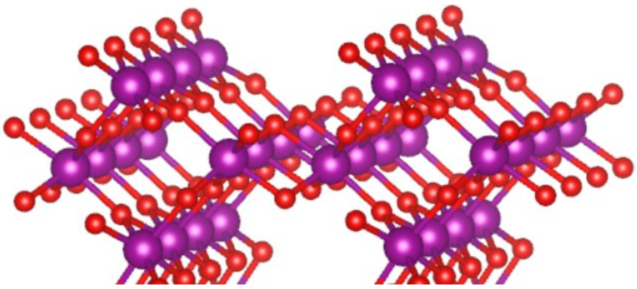

Fig. S12 Simulation model of OMS-2.

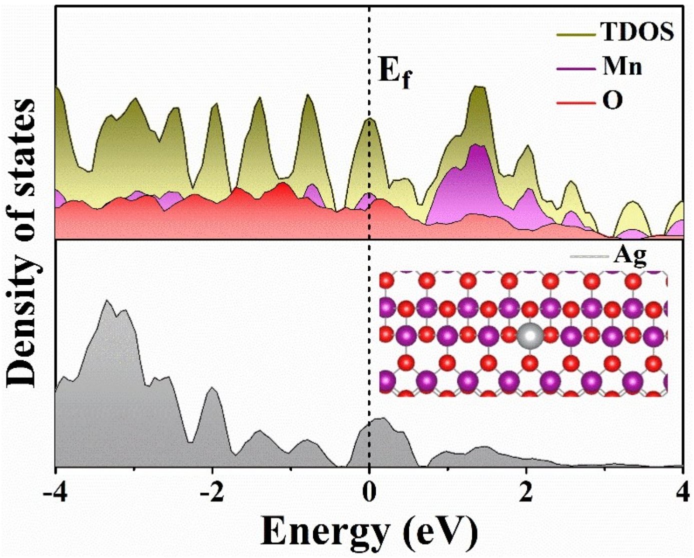

Fig. S13 TDOS and PDOS of Ag_1/OMS-2. Inset: schematic model.

Actually, the OMS system is difficult to simulate as the d electrons related magnetic properties of manganese. The authors have considered the DFT+U methods. As the authors find that the magnetic ordering of the surface structure of this system is ferromagnetism, thus, the DOS shows no band gap in the results.

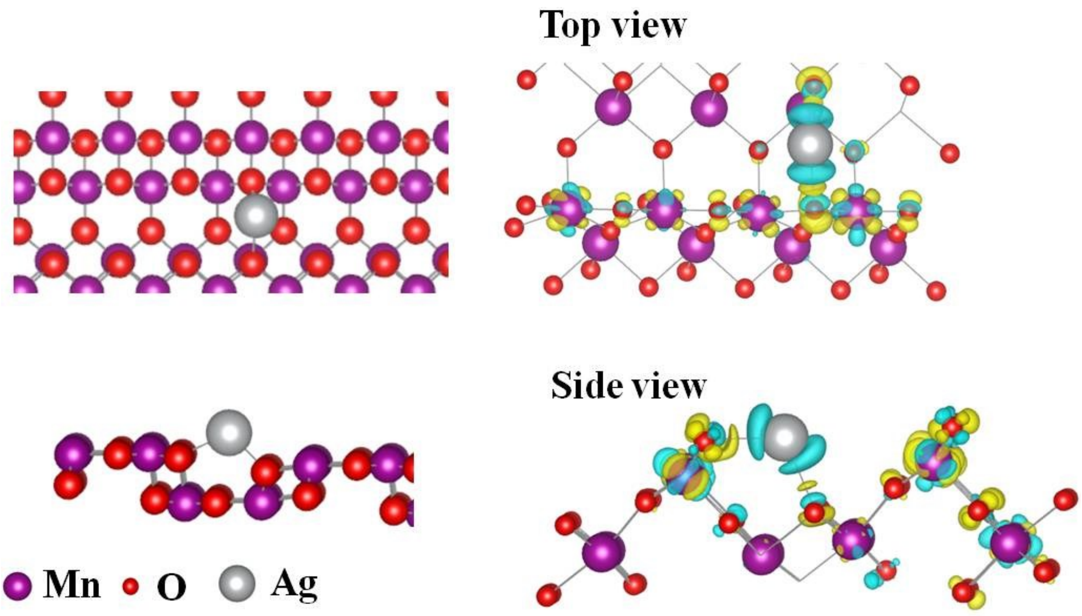

Fig. S14 Top and side views of the most stable structure and charge density difference for the Ag atom supported on the OMS-2 without Mn vacancies. Yellow and cyan regions represent electron accumulation and depletion, respectively.

Phenylacetaldehyde: ^{1}H NMR (600 MHz, CDCl$_3$): δ 9.74 (t, 1H, CHO), 7.38-7.18 (m, 5H, aromatic), 3.68 (d, 2H, CH$_2$); ^{13}C NMR (150 MHz, CDCl$_3$): δ 199.6, 131.9, 129.7, 129.1, 127.5, 50.7.

Benzaldehyde: ^{1}H-NMR (600 MHz, CDCl$_3$) δ 7.41(d, 2H, aromatic), 7.52 (t, 1H, aromatic), 7.79 (d, 2H, aromatic), 9.85 (1H, CHO); ^{13}C-NMR (150 MHz, CDCl$_3$) δ 129.34 (CH/CH), 129.74 (CH/CH), 134.57 (CH), 136.09 (C), 192.87 (CHO).

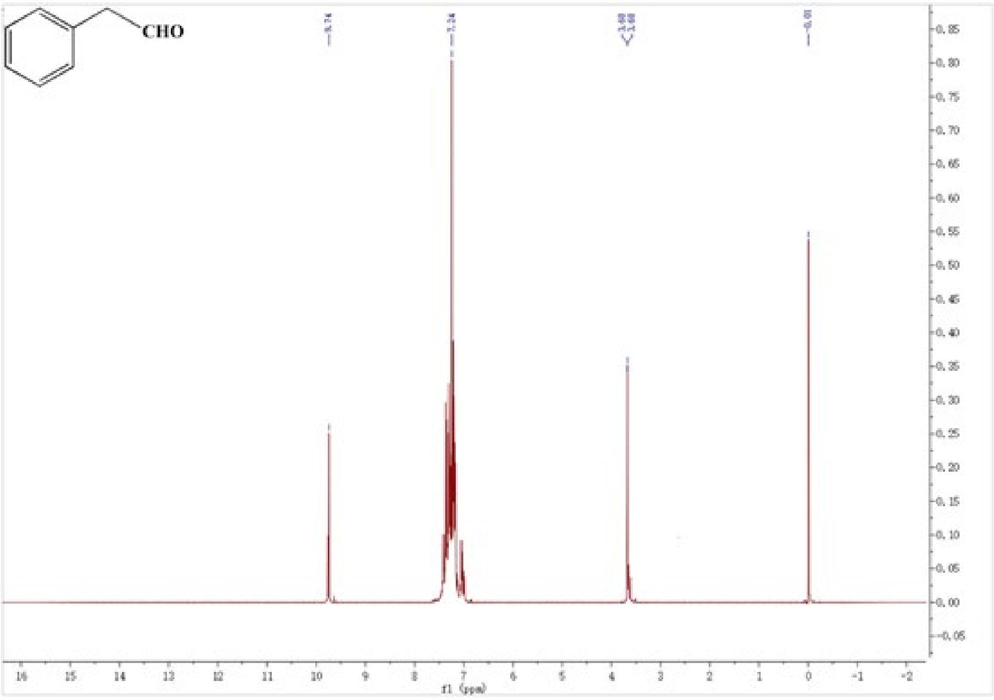

Fig. S15 ^{1}H NMR spectrum of phenylacetaldehyde.

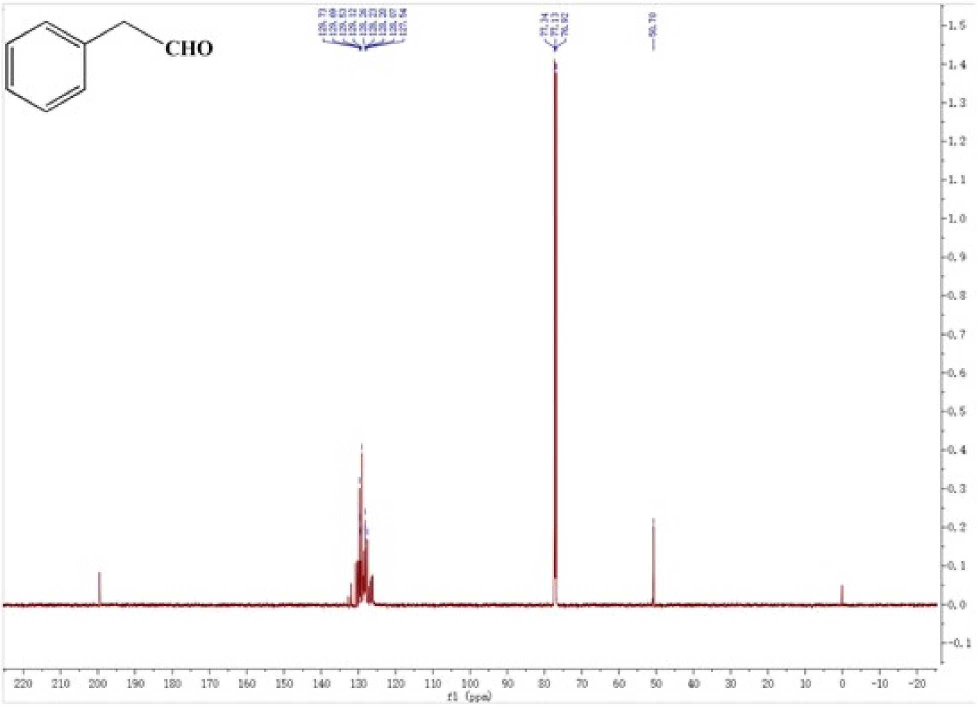

Fig. S16 ^{13}C NMR spectrum of phenylacetaldehyde.

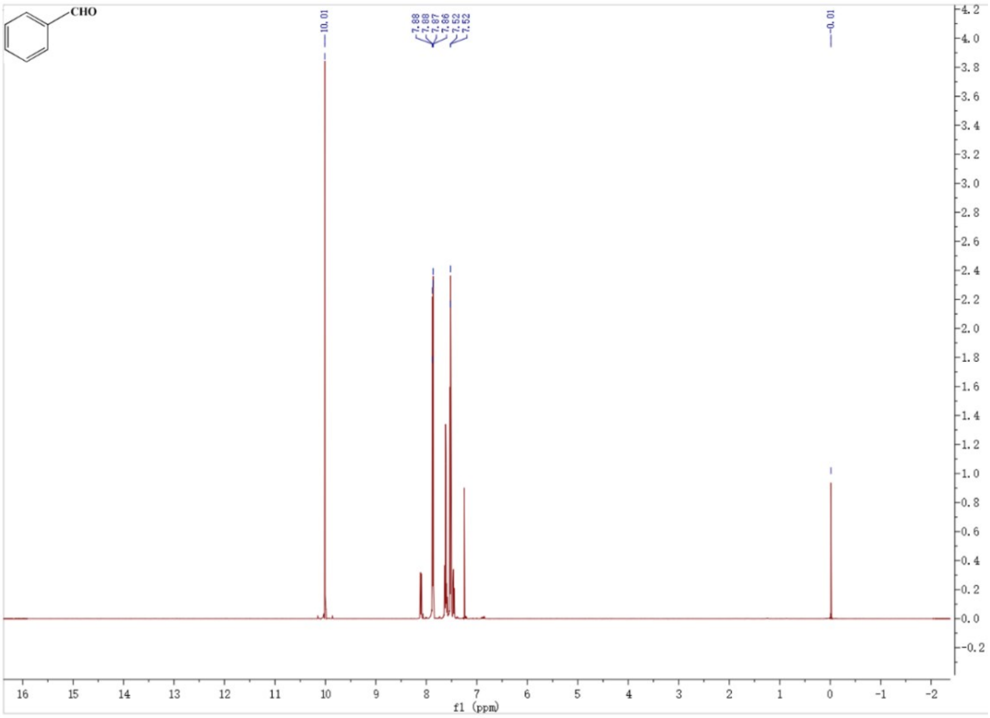

Fig. S17 ^{1}H NMR spectrum of benzaldehyde.

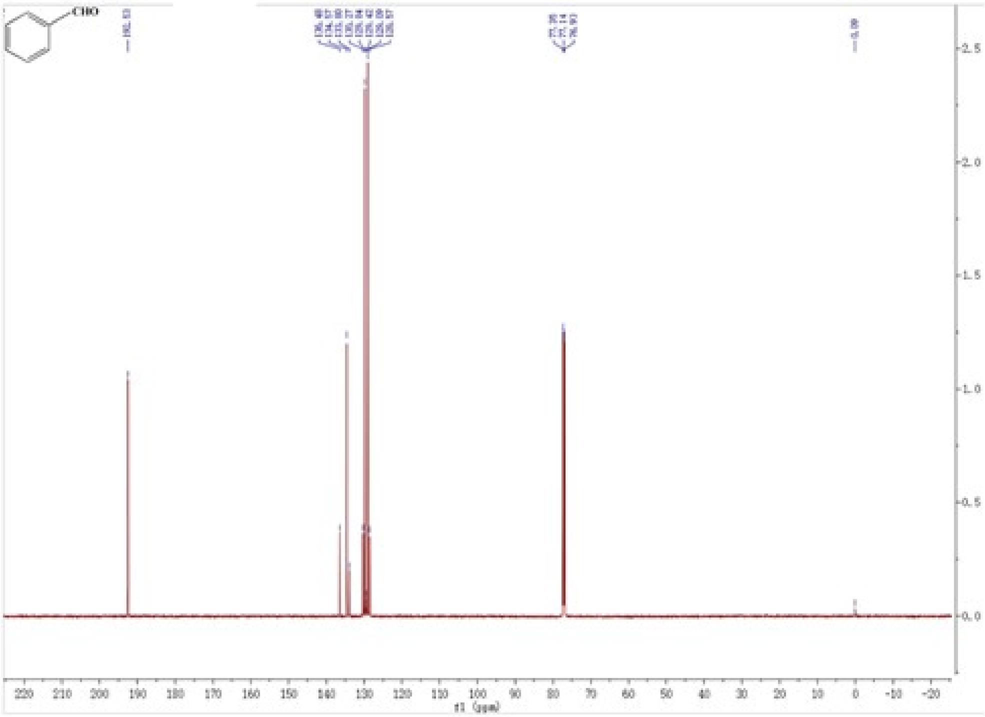

Fig. S18 ^{13}C NMR spectrum of benzaldehyde.

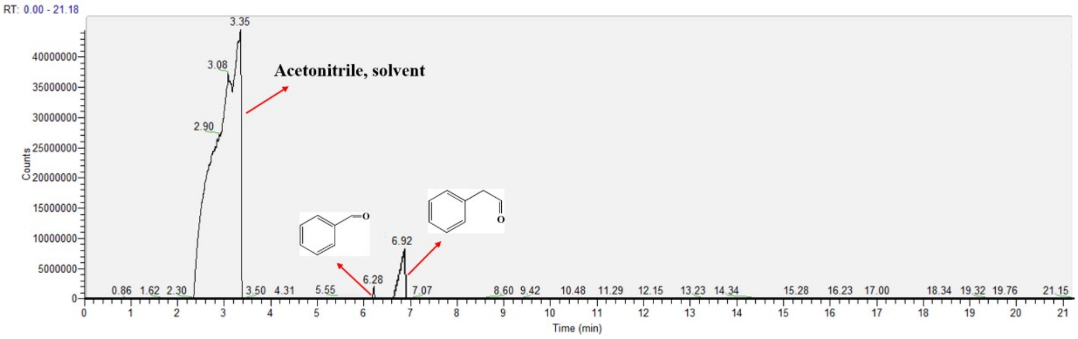

Fig. S19 GC spectrum of the product of Wacker oxidation of styrene catalyzed by Ag_1/OMS-2.

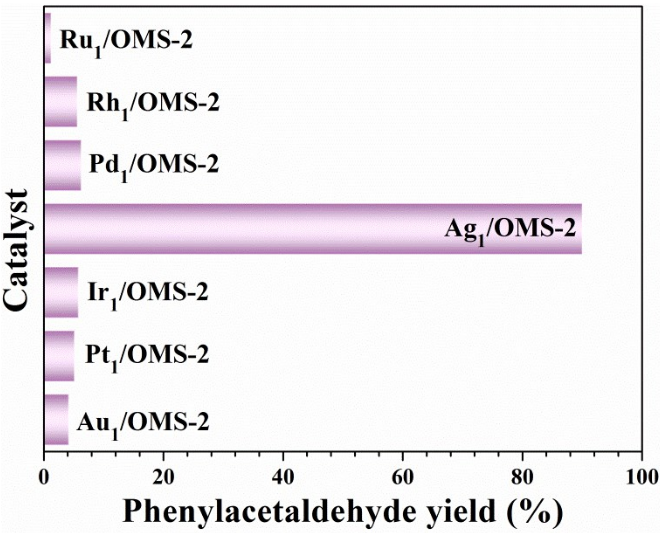

Fig. S20 Phenylacetaldehyde yield over various catalysts.

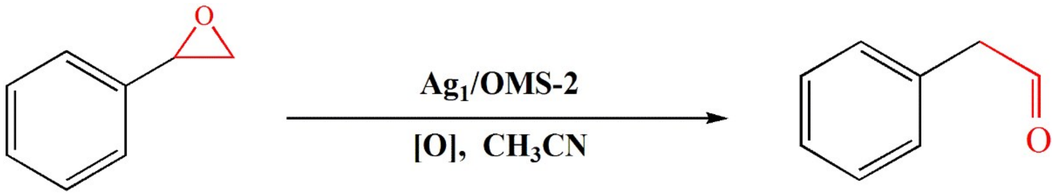

Fig. S21 Scheme of the transformation of styrene oxide to phenylacetaldehyde.

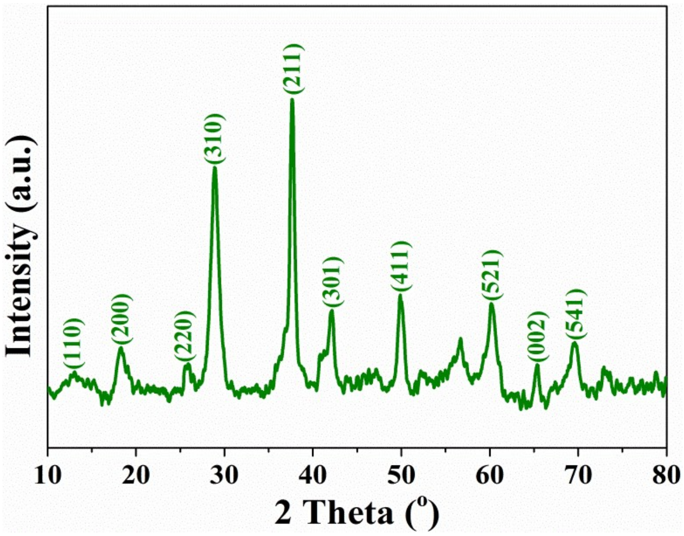

Fig. S22 XRD pattern of the spent Ag_1/OMS-2.

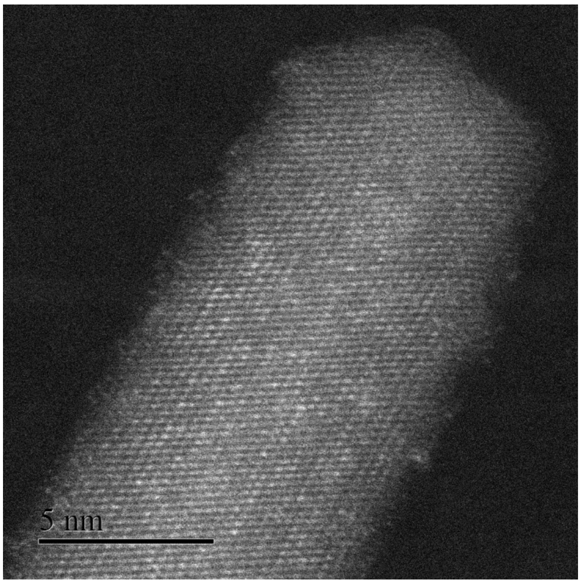

Fig. S23 HAADF-STEM image of the spent Ag_1/OMS-2 catalyst after cycling tests.

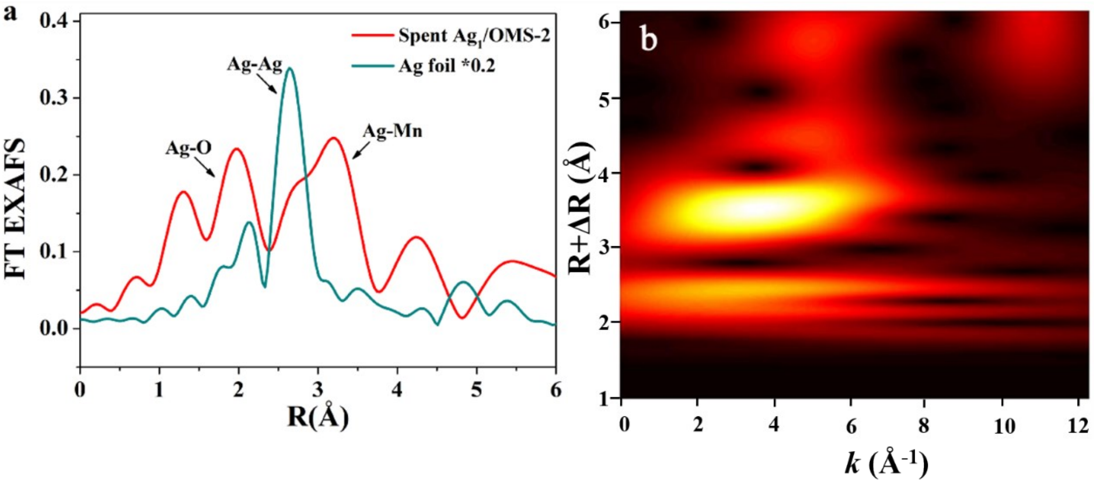

Fig. S24 a EXAFS spectrum of the spent Ag$_1$/OMS-2, **b** WT for the EXAFS signals in the spent Ag$_1$/OMS-2 (Note: Because the synchrotron radiation signals of silver and manganese interfere with each other, the quality of the measured spectrum is not very good. It has been measured many times and there is no better way to get a high-quality spectrum).

There is no intensity maximum detected near 8.5 Å^{-1} (indexed to the Ag−Ag path), confirming that no Ag particles formed after the Wacker oxidation of styrene.

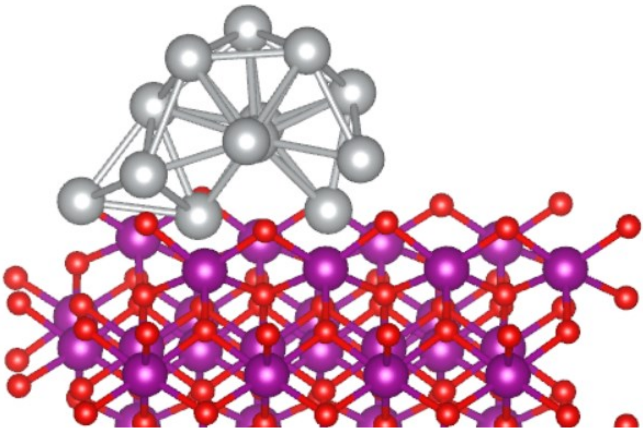

Fig. S25 The optimized structure of Ag nanoparticles.

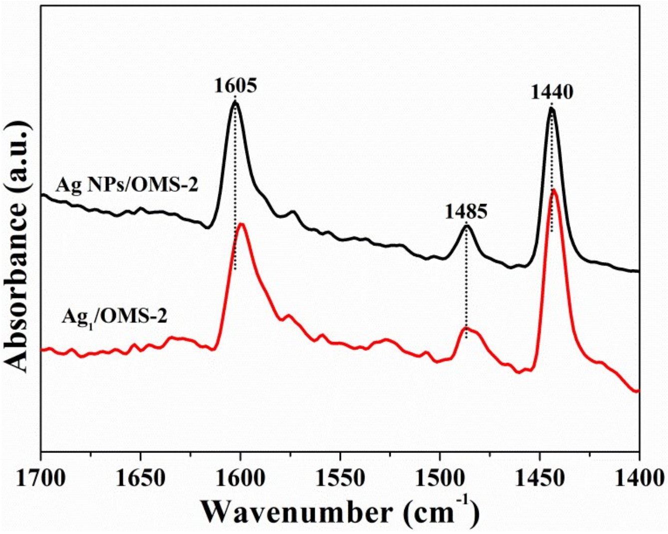

Fig. S26 Pyridine FT-IR spectra of Ag_1/OMS-2 and Ag NPs/OMS-2.

The band at ~1440 cm^{-1}can be assigned to pyridine adsorbed on Lewis acid sites, and the intensity of this peak for Ag_1/OMS-2 is larger than that of the Ag NPs/OMS-2. The absence of a peak around 1550 cm^{-1}indicates the lack of strong Brønsted acid sites. However, the peak at ~1605 cm^{-1} denotes hydrogen-bonded pyridine, which implies very weak Brønsted acidity. Thus, the catalyst has a dominant Lewis acidity, most probably associated with the Mn^{4+}/Mn^{2+} couple.[14]

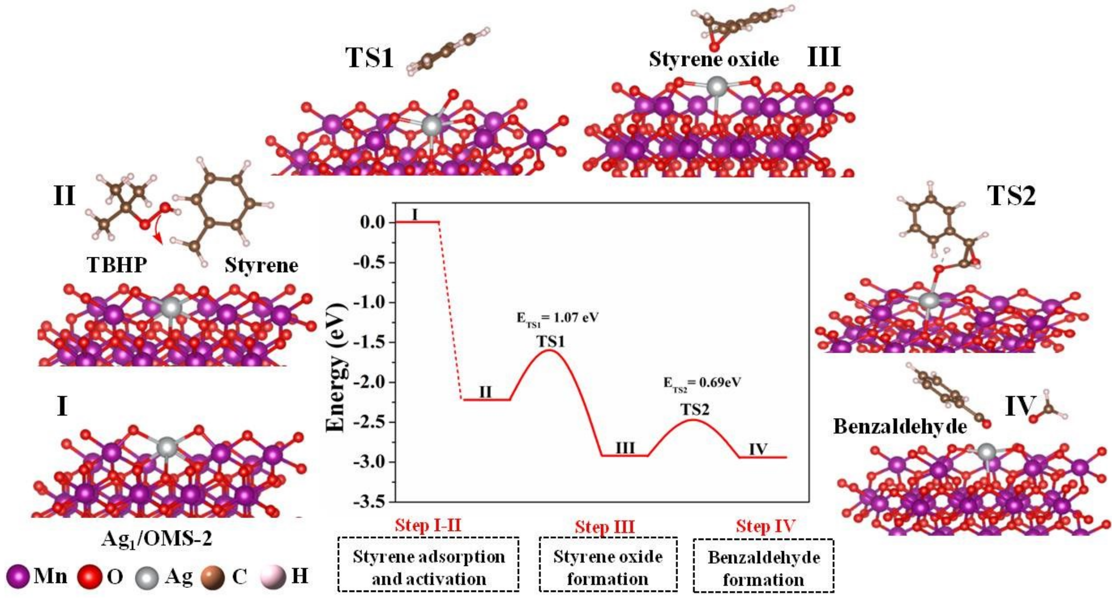

Fig. S27 DFT calculations proposed a reaction pathway for the side reaction process for Wacker oxidation of styrene to benzaldehyde on Ag_1/OMS-2, and the calculated energy profiles.

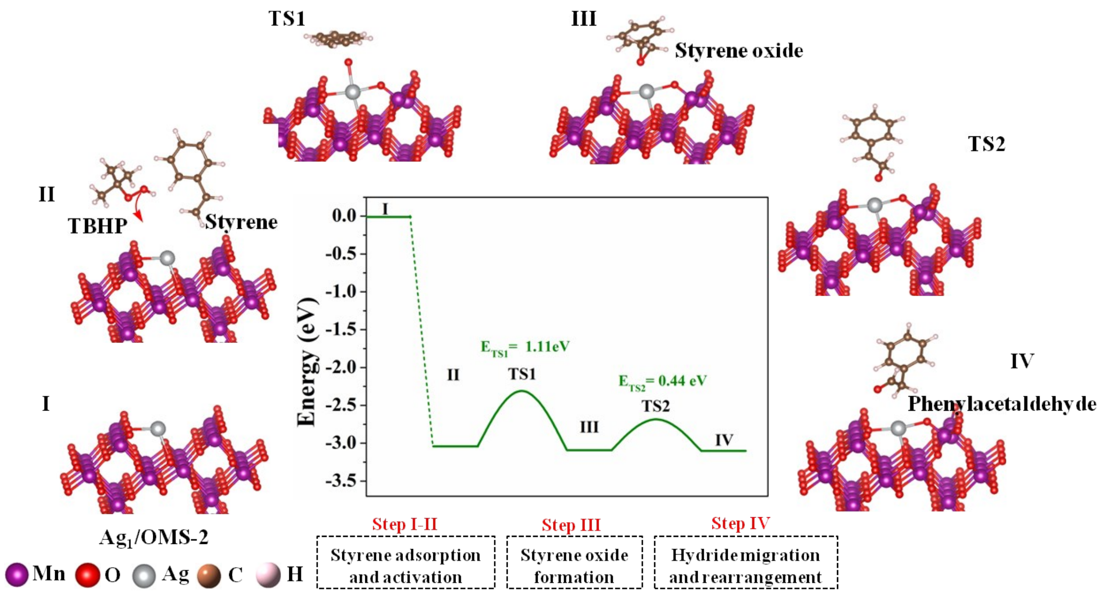

Fig. S28 DFT calculations proposed a reaction pathway for Wacker oxidation of styrene over single Ag atoms supported on the OMS-2 nanorods, and its calculated energy profiles.

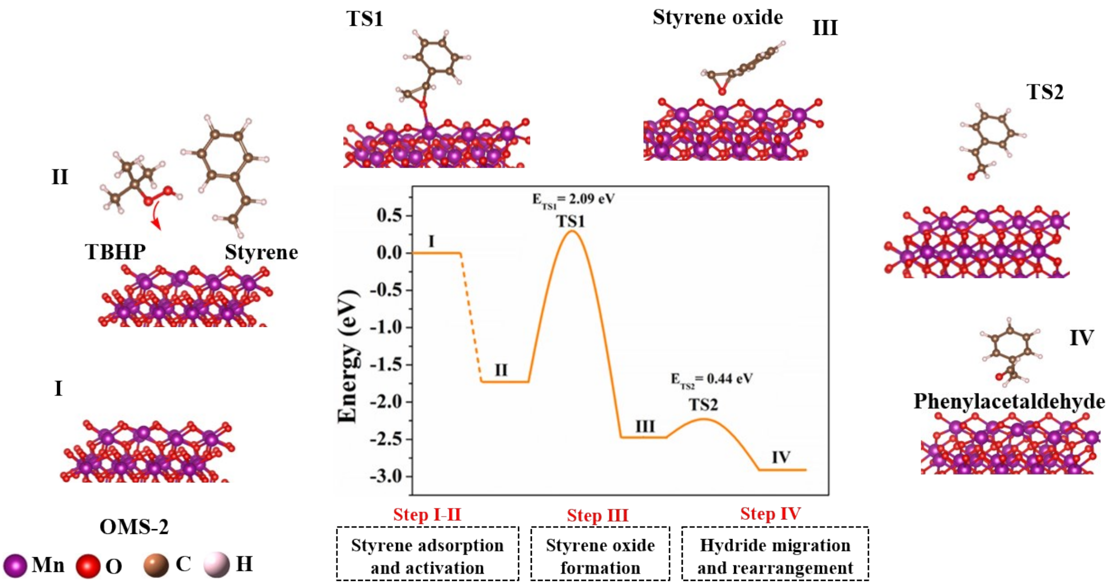

Fig. S29 DFT calculations proposed a reaction pathway for Wacker oxidation of styrene over OMS-2 nanorods， and its calculated energy profiles.

Table S1 Positron lifetime parameters of OMS-2 and Ag_1/OMS-2.

Sample	τ_1 (ps)	τ_2 (ps)	τ_3 (ps)	I_1 (%)	I_2 (%)	I_3 (%)
OMS-2	190.4±6.1	367.6±6.4	2002±97	39.0±2.1	59.1±2.1	1.9±0.1
Ag_1/OMS-2	174.5±2.2	351.5±3.5	1903±68	40.9±1.0	57.1±0.9	2.0±0.1

Table S2 Structural parameters of catalysts.

Catalyst	S_{BET}[a] (m^2/g)	V_p[b] (cm^3/g)	D[c] (nm)
Ag_1/OMS-2	79	0.58	22
OMS-2	82	0.59	23

[a] Total surface area determined by the BET method.

[b] Total pore volumes obtained at p/p_0 = 0.99.

[c] Pore size determined from the desorption branch using the DFT method.

Table S3 XPS survey of as-made OMS-2 and Ag_1/OMS-2.

Sample	Mn 3*s* (eV)			Average Mn oxidation state[c]
	BE_1[a]	BE_2[a]	ΔE[b]	
OMS-2	89.51	84.57	4.94	3.39
Ag_1/OMS-2	89.15	84.33	4.82	3.53

[a] Binding energy of two chemical states were obtained for Mn 3*s* photoelectrons.

[b] $\Delta E = BE_1 - BE_2$ of Mn 3*s* photoelectrons.

[c] Average Mn oxidation state = $8.956 - 1.126 * \Delta E$

Table S4 Structural parameters of Ag_1/OMS-2, Ag foil and AgO extracted from the EXAFS fitting. (S_0^2=0.85)

Sample	Scattering pair	CN	R(Å)	σ^2(10^{-3}Å^2)	ΔE_0(eV)	R factor
Ag_1/OMS-2	Ag-O	4	2.06±0.02	6.3±0.5	-5.6±0.5	0.01
	Ag-Mn	4.6±0.7	3.72±0.02	7.8±0.6	-6.2±0.6	0.01
Ag foil[15]	Ag-Ag	12	2.86	9.5	-	-
AgO[15]	Ag-O	1.9	2.03	3.5	-	-
	Ag-Ag	11.5	3.36	17.6	-	-

S_0^2 is the amplitude reduction factor; CN is the coordination number; R is interatomic distance (the bond length between central atoms and surrounding coordination atoms); σ^2 is Debye-Waller factor (a measure of thermal and static disorder in absorber-scatterer distances); ΔE_0 is edge-energy shift (the difference between the zero kinetic energy value of the sample and that of the theoretical model). R factor is used to value the goodness of the fitting.

Table S5 Wacker oxidation of alkenes catalyzed by Ag$_1$/OMS-2 catalyst.[a]

Entry	Substrate	Product	Conv./%[b]	Sel./%[b]	Yield/%[b]
1	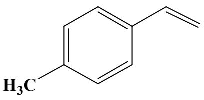	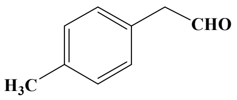	100	92	92
2	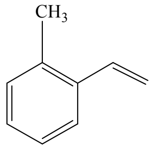	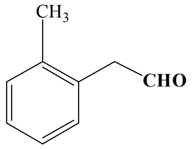	100	90	90
3	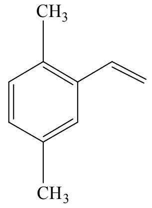	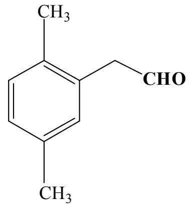	100	91	91
4	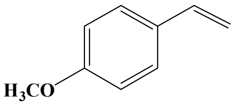	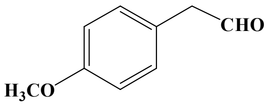	100	90	90
5	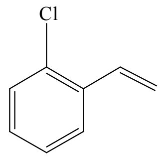	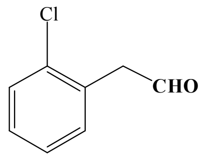	100	89	89
6	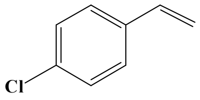	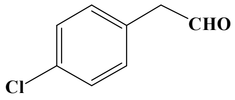	98	93	91
7	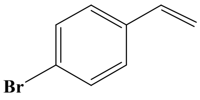	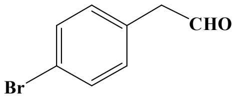	96	94	90
8	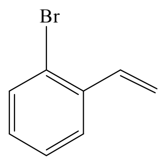	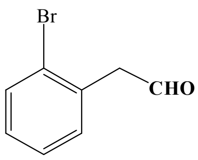	97	93	90
9	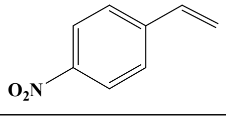	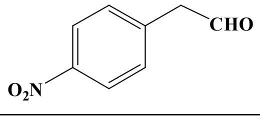	100	90	90

[a] Reaction conditions: substrate (10.5 mmol), 15 mmol TBHP, 20 mg catalyst, 20 mL CH_3CN, 80 °C, 10h.

[b] Determined by GC and GC-MS.

Table S6 Reaction conditions and catalytic performances for oxidation of styrene over Ag_1/OMS-2, in comparison with the breakthroughs in recent years.

Catalyst	Yield (%)[a]	TOF (h^{-1})[b]	TON [c]	Product Selectivity (%)				Reference	Type of Catalytic system
				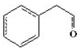	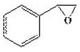	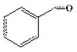	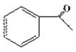		
Ag_1/OMS-2	90	1038	578	90	0	10	0	This work	Heterogeneous
Au_{55}/BN	0	108	0	0	14	82	4	*Nature*,2008[16]	
Au/CNT	0	-	0	0	2.5	14	0	*J. Am. Chem. Soc.*,2011[17]	
Fe/CN	0	-	0	0	89	11	0	*Adv. Mater.*, 2020[18]	
N-Graphene	0	-	0	0	45	54	0	*Angew. Chem. Int. Ed.*, 2018[19]	
Ru(IV)	99	-	0.01	99	0	0	0	*Angew. Chem. Int. Ed.*,2004[20]	Homogeneous
Pd(II)	83	37	-	98	-	-	-	*Org. lett.*,2012[21]	
Fe-P450	-	-	-	81	19	-	-	*Science*,2017[22]	Enzymatic

[a] Phenylacetaldehyde yield = styrene conversion × phenylacetaldehyde selectivity × 100%.

[b] Turnover frequency (TOF) = moles of styrene converted per mole of Ag in the catalyst per hour.

[c] Turnover number (TON) = moles of phenylacetaldehyde produced per mole of Ag in the catalyst, the results calculated from the references did not exclude the contribution of supports.

References

[1] F. Tuomisto, *Rev. Mod. Phys*. **2013**, *85*, 1583–1632.

[2] C. Ophus, *Adv. Struct. Chem. Imaging* **2017**, *3*, 92−101.

[3] K. Momma, F. Izumi, *J. Appl. Crystallogr*. **2011**, *44*, 1272−1276.

[4] B. Ravel, M. Newville, *J. Synchrotron Radiat*. **2005**, *12*, 537−541.

[5] M. R. Knecht, M. G. Weir, A. I. Frenkel, R. M. Crooks, *Chem. Mater*. **2008**, *20*, 1019−1028.

[6] Y. Joly, *Phys. Rev. B* **2001**, *63*, 125120.

[7] O. Bunău, Y. Joly, *J. Phys. Condens. Matter*. **2009**, *21*, 345501.

[8] M. Boudart, *Chem. Rev*. **1995**, *95*, 661-666.

[9] G. Kresse, J. Furthmüller, *Comput. Mater. Sci*. **1996**, *6*, 15−50.

[10] G. Kresse, J. Furthmüller, *Phys. Rev. B: Condens. Matter Mater. Phys*. **1996**, *54*, 11169−11186.

[11] P. E. Blochl, *Phys. Rev. B* **1994**, *50*, 17953−17979.

[12] J. P. Perdew, K. E. M. Burke, *Phys. Rev. Lett*. **1997**, *78*, 3865–3868.

[13] B. J. Delley, *Chem. Phys*. **1990**, *92*, 508–517.

[14] Makwana, V. D. *J. Catal*. **2002**, *210*, 46–52.

[15] X. H. Jiang, L. S. Zhang, H. Y. Liu, D. S. Wu, F. Y. Wu, L. Tian, L. L. Liu, J. P. Zou, S. L. Luo, B. B. Chen, *Angew. Chem. Int. Ed*. **2020**, *59*, 1–6.

[16] M. Turner, V. B .Golovko, O. P. H. Vaughan, P. Abdulkin, A. Berenguer-Murcia, M. S. Tikhov, B. F. G. Johnson, R. M. Lambert, *Nature*, **2008**, *454*, 981−984.

[17] L. Alves, B. Ballesteros, M. Boronat, J. R. Cabrero-Antonino, P. Concepcion, A. Corma, M. A. Correa-Duarte, E. J. Mendoza, *Am. Chem. Soc*. **2011**, *133*, 10251–10261.

[18] Y. Xiong, W. M. Sun, P. Y. Xin, W. X. Chen, X. S. Zheng, W. S. Yan, L. R. Zheng, J. C. Dong, J. Zhang, D. S.Wang, Y. D. Li, *Adv. Mater*. **2020**, 2000896−2000904.

[19] G. D. Wen, Q. Q. Gu, Y. F. Liu, R. Schlçgl, C. X. Wang, Z. J. Tian, D. S. Su, *Angew. Chem. Int. Ed*. **2018**, *57*, 16898–16902.

[20] J. Chen, C. M. Che, *Angew. Chem. Int. Ed*. **2004**, *43*, 4950 –4954.

[21] P. L. Teo, Z. K. Wickens, G. B. Dong, R. H. Grubbs, *Org. lett*. **2012**, *14*, 3237–3239.

[22] S. C. Hammer, G. Kubik, E. Watkins, S. Huang, H. Minges, F. H. Arnold，*Science*. **2017**, *358*, 215−218.